PRESSURE DISTRIBUTION DUE TO STERN TAB DEFLECTION AT MODEL SCALE

(DOI No: 10.3940/rina.ijme.2015.a1.303)

T Arnold, J Lavroff and **M R Davis,** University of Tasmania, Australia

SUMMARY

Trim tabs form an important part of motion control systems on high-speed watercraft. By altering the pitch angle, significant improvements in propulsion efficiency can be achieved by reducing overall resistance. For a ship in heavy seas, trim tabs can also be used to reduce structural loads by changing the vessel orientation in response to encountered waves. In this study, trials have been conducted in the University of Tasmania hydraulics laboratory using a closed-circuit water tunnel to measure model scale trim tab forces. The model scale system replicates the stern tabs on the full-scale INCAT Tasmania 112 m high-speed wave-piercer catamaran. The model was designed for total lift force measurement and pressure tappings allowed for pressures to be measured at fixed locations on the underside of the hull and tab. This investigation examines the pressures at various flow velocities and tab deflection angles for the case of horizontal vessel trim. A simplified two-dimensional CFD model of the hull and tab has also been analysed using ANSYS CFX software. The results of model tests and CFD indicate that the maximum pressure occurs in the vicinity of the tab hinge and that the pressure distribution is long-tailed in the direction forward of the hinge. This accounts for the location of the resultant lift force, which is found to act forward of the tab hinge.

LIST OF SYMBOLS

α	Tab deflection angle [degrees, positive up]
N	Water tunnel pump speed [RPM]
k	Pressure transducer linear calibration constant [Pa V^{-1}]
P	Measured pressure across a transducer [Pa]
P_t	Flow total pressure [Pa]
P_s	Flow static pressure [Pa]
s	Sinkage of test model [m, positive down]
y	Flow depth [m]
U	Flow velocity [m s^{-1}]
x	Location relative to tab hinge [m]
V	Pressure transducer output voltage [V]
V_0	Pressure transducer zero pressure voltage [V]
ρ	Density of water [kg m^{-3}]

ABBREVIATIONS

CFD	Computational fluid dynamics
$RANS$	Reynolds Averaged Navier-Stokes
RMS	Root mean square
SST	Shear Stress Transport

1. INTRODUCTION

High-speed catamarans have the ability to carry high loads at faster speeds than is otherwise possible due to their stability and hull slenderness. The use of high-speed wave-piercing catamarans is therefore favoured for their superior efficiency and seakeeping characteristics compared with monohull designs [1]. Performance of these vessels is an area of continual improvement as new information and research becomes available. The optimisation of vessel performance combines the objectives of reducing motion resistance by adjustment of vessel trim and so increasing propulsion efficiency, and also of reducing structural weight to increase structural efficiency. Stern tabs can contribute significant benefits in both aspects, allowing vessel trim to be optimised on a continuous basis whilst also reducing undesirable ship motions at high speed and so increasing passenger comfort. Motion controls thus provide a means of performance optimisation and simultaneous improvement of passenger comfort during high speed ship travel especially during operation under adverse sea and weather conditions.

Trim tabs are primarily used to control the pitching motion and pitch trim of a moving vessel, which can reduce the overall vessel resistance. The pitch of a ship can be somewhat influenced by forward velocity due to the hydrodynamic lift force on the hull, which creates a hydrodynamic moment about the transverse axis [2]. On a catamaran with a trim tab on each hull, the tabs can also be operated to counteract rolling. Previous studies of motion controls such as T-foils and trim tabs [3, 4] have investigated the subsequent effect on vessel pitch trim angle, rather than measuring the actual loads created by the tabs and foils.

The magnitude and location of the resultant force due to trim tab deflection and the subsequent lift coefficient have been investigated by Bell [5] and Arnold [6]. Following these studies, there is an evident need to understand how the hull pressure due to tab deflection is distributed. The quantification of loads produced by trim tab deflection provides the basis for the design of tabs as a form of ride control. If the pitch trim correcting moment due to unsteady tab deflection is known, then more accurate design of motion control systems becomes possible. Also, there is an optimum tab angle which achieves minimum drag on a vessel at a given speed due to the influence of the tab on the pitch trim angle [4]. Knowledge of the pressure distribution caused by trim tab deflection also provides insight into the structural stresses which are created on the ship by trim tab operation. It is important to understand the structural loads on a vessel so that the structure is of adequate strength without being over-designed [7].

Structural loads on a ship moving through waves are dependent on the height, frequency and direction of the encountered waves and the forward speed of the vessel. Structural loads are more significant for high speed vessels with high length Froude numbers. High speed catamarans generally operate at length Froude numbers of 0.7 or above and this leads to increased ship motions [8]. The maximum forces exerted on the structure of a ship occur during slamming events, in which the water surface impacts the underside of the vessel during large motions. The resulting short duration high structural loads give rise to a vibratory whipping response for high-speed catamarans as investigated by Lavroff [9], Thomas [10] and Davis et al. [11]. Maximum wave loads have been found to be of the same magnitude or greater than the ship weight. There is therefore a strong incentive to reduce ship motions for reasons of structural loading as well as passenger comfort.

It has been found that the resultant force from trim tab deflection is located forward of the tab hinge [6]. Tsai et al. [3] identified that tab deflection creates an upstream region of pressurised flow underneath the hull. The present investigation examines in detail the pressure distribution in the region of flow underneath the tab and hull. A CFD analysis has been carried out in conjunction with experimental model testing to support and verify the CFD procedure. CFD analysis allows modelling of ship dynamics to a high level of detail and with great flexibility which cannot easily be matched by experimental measurement programmes. Multiple aspects of a ship can be studied individually and together, as demonstrated by Sridhar et al. [12].

The best representation of flow under the tab and hull would include a complete three-dimensional model of the hull and tab. However, to provide an indication of the streamwise pressure distribution, the present investigation applies CFD analysis to a simplified two-dimensional model of the flow under the hull and tab. The model test results obtained in this present investigation will also provide an indication of the pressure distribution along the hull centerline under three dimensional conditions with a finite width tab on which pressure tappings are located and for which the entire aft section of the hull and tab are mounted so as to allow measurement of the location and magnitude of the total lift force due to the tab deflection.

The experimental measurements and CFD analysis were both conducted at model scale. A tab scale of 1:44.8 was used for the investigation, which replicates the tabs on the 2.5 m segmented catamaran model used by Lavroff [9]. The upstream apparatus length does not comply with either Reynolds number or Froude number similarity with the full scale vessel. Due to jet intakes located on the underside of each hull on the 112 m INCAT catamaran, the flow conditions entering the undisturbed stern hull section are unknown. For this reason, any length-based similarities are of little significance as the boundary layer development is interrupted. Therefore no attempt has been made to model the incident hull boundary layer at the tab. In fact the test model (Figure 1) is relatively short and so was considered to have a relatively thin hull boundary layer at the tab, as would be the case where an upstream water jet intake has drawn off the hull boundary layer ahead of the trim tab mounted on the hull transom.

2. MODEL AND TEST APPARATUS

Testing was conducted in the closed circuit circulating water tunnel in the University of Tasmania Hydraulics Laboratory, shown below in Figure 2. The water tunnel is usually operated completely full of water and drained of air, with a closed working section. For this experiment, the working section was open and the water level was lowered below that of the tunnel roof. The working section has a length of 1000 mm, a width of 600 mm and a usable depth of 200 mm for this application.

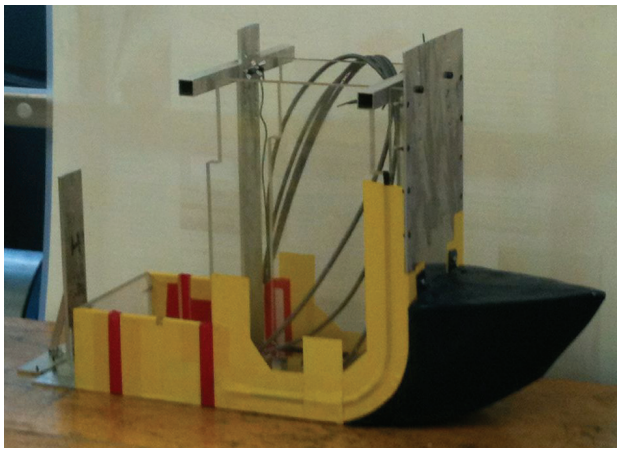

Figure 1: Model scale apparatus without pressure lines attached.

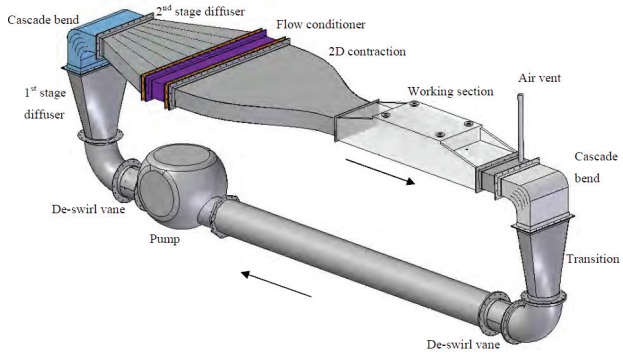

Figure 2: University of Tasmania water tunnel (from Barton [13]).

Due to flow instability when operating with an open test section at higher velocities, a modification to the existing facility was required to achieve a suitable flow quality over the desired velocity range. A flow constriction flap was installed on the upstream edge of the test section to accelerate the flow and achieve suitable flow velocities at a shallower depth. The constriction flap in operation is shown in Figure 3.

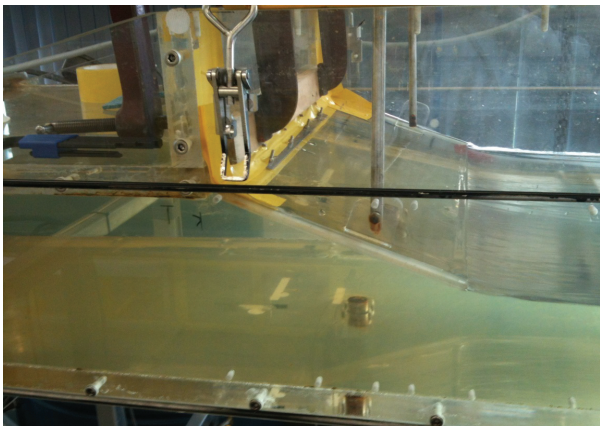

Figure 3: Flow constriction flap in the water tunnel. Flow is left to right, upstream surface meets flap near to its mid-point.

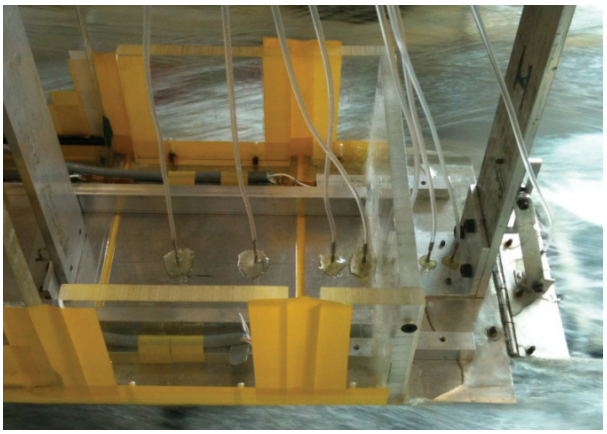

Figure 4: Pressure tappings on centre line of model test apparatus in water tunnel.

Simulation of the flow underneath a catamaran hull was performed at model scale with the same apparatus as used by Bell [5] and Arnold [6] using the same trim tab dimensions as given in Table 1. Due to flexure in the apparatus' segmented hull which is required for force measurement using strain gauges, maintaining level trim at the transom edge for all trials was a difficult task. As no strain gauge readings were taken in these tests, additional stiffening linkages were attached to the segmented hull to prevent any significant flexure in the segmented hull. Pressure tappings, shown in Figure 4, were added at various locations along the hull centreline. The placement of these tappings was restricted by the location of existing fixtures on the apparatus. The tapping locations are detailed in Table 2.

Table 1: Model scale trim tab dimensions.

Effective length (hinge centre to trailing edge) (m)	0.037
Trim tab width (m)	0.130

Table 2: Pressure tapping locations forward of tab hinge (negative values define position forward of tab hinge, positive values define position aft of tab hinge).

Tapping no.	**Location *x* from tab hinge**
1	-205 mm
2	-155 mm
3	-105 mm
4	-85 mm
5	-65 mm
6	-45 mm
7	-30 mm
8	20 mm

2.1. INSTRUMENTATION & CALIBRATION

Pressure measurement was conducted using Validyne DP15 Variable Reluctance Differential Pressure Transducers, which implement a differential measurement of pressures either side of a diaphragm. The DP15 signal was sent to a Validyne CD15 Carrier Demodulator. Following the CD15 was a current-to-voltage converter, from which the signal was sent to a National Instruments SCB-100 terminal block for data acquisition. The input and output ports on the SCB-100 were controlled and read using LabView interfaces. One transducer was used to measure flow velocity using a pitot-static probe, whilst the other was used to sample the static pressures from the tappings on the underside of the hull using solenoid operated valve selectors. The output voltages from the two pressure transducers were read as differential analogue inputs.

Calibration of the pressure transducers was carried out using known differences in pressure across the transducer and recording the output voltages. The pressure differences were created using two columns of water to generate a static pressure head. The tubes could be equalised by opening a connecting valve or isolated by closing the valve. The linear relationship between pressure and voltage is given in Equation 1. It is assumed that whilst the zero voltage V_0 may drift over time, the proportional relationship k between pressure and voltage remains constant. Calibration data for both pressure transducers is shown graphically in Figure 5 and Figure 6 and the linear calibration represented by

$$P = kV - V_0. \qquad (1)$$

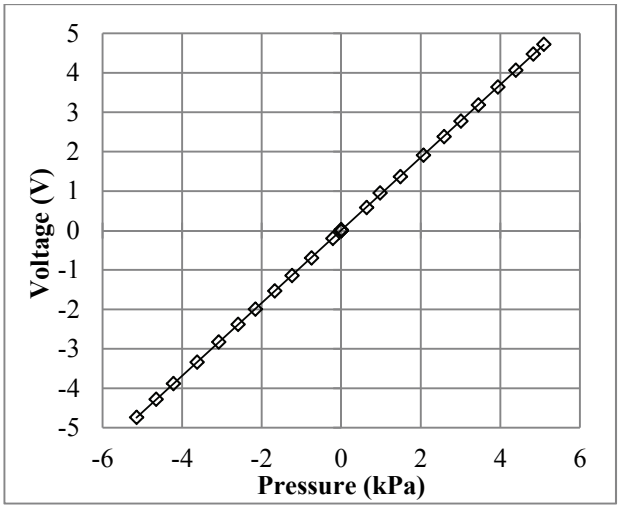

Figure 5: Velocity pressure transducer calibration.

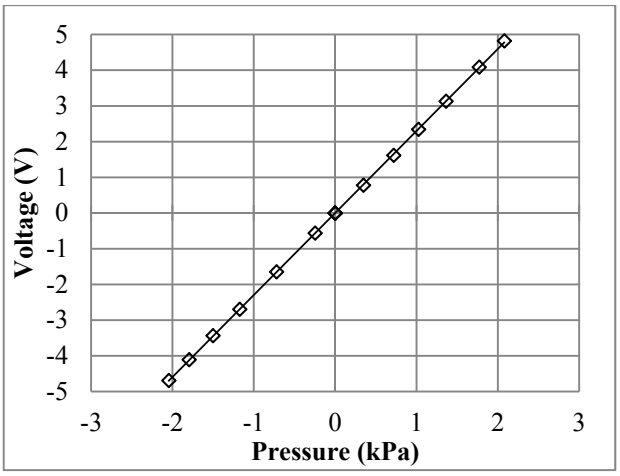

Figure 6: Hull pressure transducer calibration.

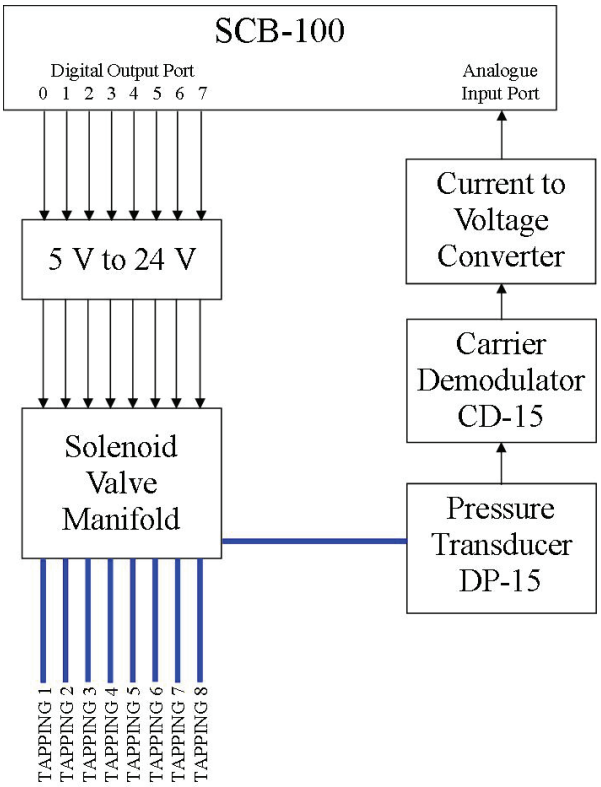

Figure 7: Hull pressure control and DAQ system schematic.

For the velocity pressure transducer, the measured pressure is the difference between static pressure and total flow pressure. This output therefore represents only the dynamic pressure component. The relationship between pressure and velocity, shown in Equation 2, is derived from the Bernoulli equation. Combining this relationship with the pressure-voltage calibration factor k in Equation 1, an expression for the flow velocity can be obtained in terms of transducer output voltage, as shown in Equation 3:

$$P_{pitot} = P_t - P_s = \frac{\rho U^2}{2} \quad (2)$$

$$U = \sqrt{\frac{2(kV - V_0)}{\rho}} \quad (3)$$

The pressures from each tapping on the apparatus hull were sampled individually in sequence using eight solenoid valves linked by a manifold. The hull pressure transducer used a static column of water on one side as an arbitrary reference pressure. This pressure does not need to be known, as it is consistent for both the tests with and without tab deflection for each flow velocity and tab angle combination. Each of the eight switches controlling the solenoid valves was operated using one of the 8-bit digital output ports on the SCB-100. An intermediate conditioning unit converted the 5 V signal to the 24 V required to operate the solenoid valve switches. A schematic of the control and data acquisition system is shown in Figure 7. The arrows represent electrical signals and solid lines represent the water-filled pressure lines.

3. TESTING AND DATA ANALYSIS

With the trim tab set at a specified angle α to the hull undersurface, the apparatus was placed in the water tunnel, aligned with the flow, levelled and clamped in place. To achieve meaningful pressure measurements, it is necessary to clear the connecting water-filled tubes of air bubbles. Using temporary purge connections in the pressure lines, most of the air bubbles can be bled from the tubes using a difference in elevation as the driving force. By opening all the solenoid valves and disconnecting each line individually, air bubbles were also removed from inside the switches and the connecting manifold. The entrainment of air bubbles in the flow was greatest at higher velocities, hence the removal of bubbles from the pressure tubes was performed at the lowest possible velocity without a hydraulic jump present in the test section. For the faster tests, the flow velocity was increased to the desired test flow conditions after the tubes had been bled of air. Following the bleeding of air from the tubes, the output line from the solenoid valve manifold was connected to the hull pressure transducer. Using the bleed screws on the transducer, this section of the pressure line and the transducer diaphragm housing was also bled of any air bubbles which were present.

The presence of bubbles in the pressure lines can cause pressure measurement errors. However, it was found that bubbles which are significantly smaller than the internal diameter of the tube and are attached to the wall have a small effect on pressure measurement. The most significant errors are caused by the bubbles which occupy the entire internal diameter of the tube, creating what is known as an air lock. As there is surface tension existing on either side of these air locks, the pressurised air within them causes a discontinuity in

the distribution of pressure along the tube. Due to the entrainment of air bubbles in the flow underneath the apparatus hull, it was very difficult to completely remove bubbles from the lines, despite thorough bleeding of the tubes. Therefore to achieve results within an acceptable error margin, all air lock bubbles were cleared from the tubes. While some bubbles much smaller than the inner diameter of the tube remained present in some tests, their effect on results is assumed to be minimal based on a preliminary investigation of this phenomenon. Most of the bubbles which remained present in the pressure lines would be present for all trials with both positive tab deflection and no tab deflection, thus further reducing the impact on the final results for the variation of pressure with tab deflection.

Each sampling sequence of hull pressures was preceded by a measurement of the flow velocity by sampling the dynamic flow pressure for 10 seconds at 1000 samples per second. The hull pressures were then measured individually in sequence by opening and closing each of the eight solenoid valves, which are controlled by the digital output ports on the SCB-100. Due to small fluctuations in the flow conditions through the test section, the pressure values used in the results are the average of a series of four simultaneous data acquisition procedures. A series of reference trials with no tab deflection at the same flow velocity were conducted immediately following the trials with specified tab deflection, without removing the apparatus from the flow. Each tapping was again sampled individually for 10 seconds at 1000 samples per second. Sampling did not begin for 10 seconds after each valve was opened to allow the pressure to settle to a constant value. Between one valve closing and the next valve opening, a 2 second delay was allowed to further reduce any dynamic effects. The sampling of data and controlling of the digital output ports was performed using a LabView program. The specified tab deflection angles which have been tested are 0, 5, 10, 15 and 20 degrees. These tab angles have all been tested at velocities of 1.5, 1.75, 2 and 2.25 m/s.

Pressures due to tab deflection are defined as the differences in pressure between the tab deflection test and the no tab deflection reference test for each tapping. Following the subtraction of the no tab test value for each specified tab deflection, the zero degree test was subtracted from all pressure distributions for direct comparison with the CFD analysis. The magnitude of the loading due to a zero degree tab orientation is dependent on the vessel sinkage, as the lift force theoretically approaches zero as the sinkage is reduced. The tendency of the flow to return to the free surface level then creates the lift force rather than downwards flow deflection as in the positive tab deflection trials.

The recorded velocities were averaged for each trial and a pressure correction factor for the intended nominal velocity was obtained. Using the assumption of pressure being proportional to the velocity squared (from Equation 2), the hull pressures can be corrected for small variations from the specified flow velocity. This assists in the direct comparison of experimental data to the CFD results. The correction formulae applied for the hull pressures is given by Equation 4:

$$P_{corr} = P_{meas} \times \left(\frac{U_{nominal}}{U_{measured}}\right)^2 \qquad (4)$$

4. TWO DIMENSIONAL CFD ANALYSIS

The three-dimensional flow around a submerged hull is complicated, particularly at the stern of the vessel. The hydrodynamics of the stern flow require a detailed and powerful computational model. To reduce this complexity, but still achieve an indicative result for the streamwise hull pressure distribution, a two-dimensional CFD model has been used. Because three-dimensional effects have been neglected, the two-dimensional pressure distribution will give the best representation of the pressures along the hull centreline. The CFD analysis has been conducted at model scale to best represent the experimental trials at the lower Reynolds number to facilitate the numerical solution. The computational model has been developed using ANSYS Design Modeller and the simulation has been performed using ANSYS CFX Solver.

A model of single element thickness in the vertical flow plane is sufficient for a two-dimensional analysis. The hull and tab were specified as no-slip walls with a surface inflation to satisfy the requirements for accurate boundary layer modelling [14]. These surfaces also had an edge sizing of 1 mm, whilst a 2.5 mm mesh was chosen for the outer mesh elements. The dimensions of the finite element model are shown in Figure 8 and the boundary conditions are detailed in Table 3. Figure 9 shows the pressure contour under the hull and tab from CFD analysis. The medium at the upper boundary aft of the tab is specified as air, whilst the inlet medium is specified as water. The outlet boundary conditions allow for a combination of air and water to facilitate flow separation from the tab at the trailing edge and the subsequent free surface as observed during all experimental tests undertaken (Figure 4). The offset pressure distribution based on the free surface height at the outlet is based on a series of iterative simulations for each case to refine the model parameters.

Table 3: CFD model boundary conditions.

Surface	Boundary type	Boundary condition	Medium
INLET	Inlet	Velocity = U m/s	Water
OUTLET	Outlet	$P_s = 0$ Pa for $z \geq d$ $P_s = \rho g(d - z)$ Pa for $z \leq d$	Air/ Water
BASE	Wall	Slip wall	-
HULL	Wall	No-slip wall	-
TAB	Wall	No-slip wall	-
OPENING	Opening	Entrainment: Relative pressure = 0 Pa	Air
SIDES	Symmetry		-

The CFX High Resolution differencing scheme was implemented for this analysis, which uses a variable blend factor to encourage convergence of results. The solver performed iterative calculations until the RMS residual values converged to less than 10^{-6}. The turbulence model used by the solver is Shear Stress Transport, which is a two-equation model based on the RANS equations. As inlet turbulence parameters are practically negligible in marine CFD applications [14], the turbulence intensity at inlet was set at 1%, which is based on the assumption of low intensity turbulence when the body of water is stationary and the ship itself is in motion. This inlet condition is dependent on the flow conditions after the jet intakes on the ship. As these flow conditions are unknown and require complex analysis to determine, the specification of detailed inlet parameters is necessarily unsupported here.

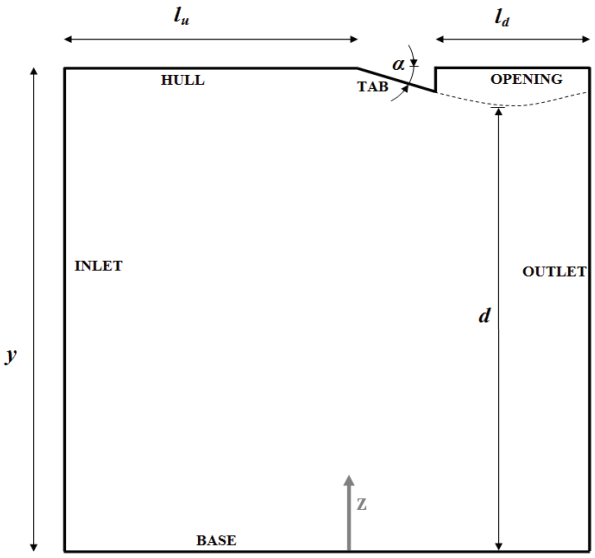

Figure 8: CFD model dimensions and labels.

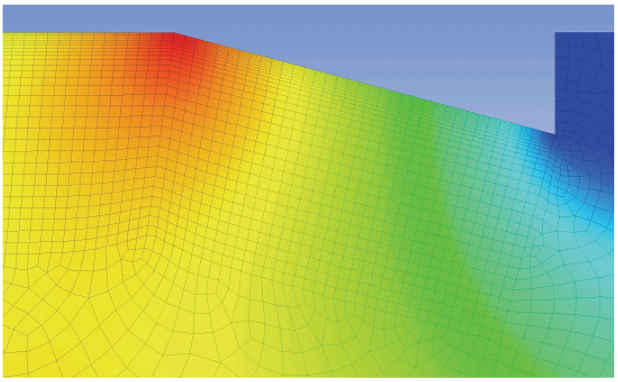

Figure 9: Example of a pressure contour under the hull and tab from CFD analysis (the colour red indicates high pressure and the colour blue indicates low pressure).

4.1 DATA CORRECTION

The two-dimensional pressure distributions obtained from CFD analysis show a non-zero upstream hull pressure as shown in Figure 10. This can be considered similar to the pressurised region upstream of flow through a nozzle. To create an upstream pressurised region, two fixed bounding surfaces are required for a two-dimensional flow. Despite only having one constricting surface, the pressurised region is created between the solid hull above and the high asymptotic hydrostatic pressure field below. As the hydrostatic pressure increases with depth, this creates an overall upward force which resists fluid displacement and hence results in a pressure increase at the hull surface.

For the physical model hull of finite width, the surrounding freestream flow reduces constriction effects and hence will prevent this pressurised region occurring laterally as in the CFD solution. Therefore, this can be assumed to be only a two-dimensional effect. The pressures on the underside of the hull can be considered as the sum of the minimum hull pressure and a varying pressure component as a function of hull position. It follows that for the three-dimensional case of a hull moving through water we would only consider the varying pressure component, as the pressurised region would not be present. Therefore, the correction applied for this pressurised region was to subtract the minimum hull pressure from the total distribution. Over the tab, a linear decay from the minimum hull pressure at the hinge to zero pressure at the trailing edge is applied. This correction method is applied to the two-dimensional CFD results, which reduces the minimum hull pressure to zero magnitude. In Figure 10, the uncorrected pressure distribution is represented by the solid line and the subtracted correction pressure is represented by the shaded region.

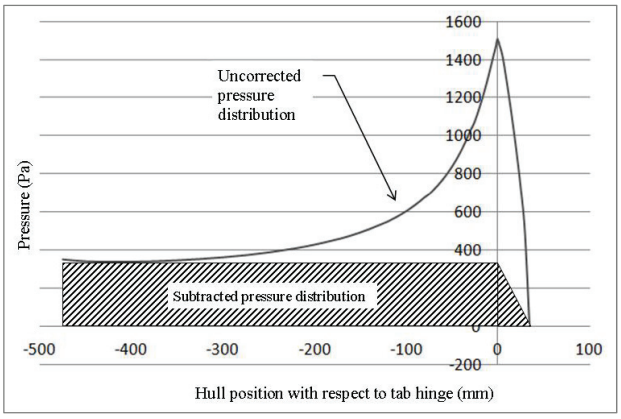

Figure 10: Pressure correction for two-dimensional effects.

5. RESULTS

Comparisons of the measured pressures and those predicted using CFD analysis are shown in Figure 11 to Figure 14. From the CFD results, the maximum pressure is shown to occur at the corner where the deflected tab joins the hull. The pressure distribution is long-tailed in the hull upstream direction, indicating that the centre of pressure is located forward of the tab. This is consistent

with previously published results for the total tab and hull force data [15].

The experimental results compare quite closely with the CFD predictions. However the magnitude of the measured pressures is slightly greater than the corresponding CFD predictions at lower velocities. It must be considered that the flow depth of 102 mm will induce some flow constriction effects. The subsequent static pressure increase due to constriction in the flow underneath the hull of the apparatus is demonstrated by the uncorrected two-dimensional CFD results. It appears that the first and second tappings, which are located furthest upstream, consistently exhibit pressures greater than the predicted CFD pressures. These tappings are the most influenced by the flow development region as the oncoming flow interacts with the bow of the apparatus, as well as the pressure increase due to constriction effects.

With no tab deflection, the transom of a hull exhibits a negative pressure gradient in order to satisfy continuity with the zero pressure condition at the trailing free surface. This negative pressure gradient has the effect of creating a moment about the transverse axis due to the relative suction pressure in the vicinity of the stern. By using the no tab trials as a reference, it can be seen how trim tabs turn the usual negative transom pressure gradient into a positive pressure gradient.

The measurement accuracy is best for the larger tab deflection angles, due to the reduction of small flow fluctuation effects. The greater lift force acting on the hull reduces the apparatus' susceptibility to hull vibration caused by small disturbances in the flow. The greater pressure magnitudes caused by large tab angles are also less affected by small variations in the flow velocity than for smaller tab angles at the same velocity.

The pressure tapping located on the tab was subject to the most variation due to unsteadiness of the flow. As the tab was deflected into the flow, small fluctuations in flow velocity had a more significant impact on the measured pressure than was the case for the tappings which were located on the hull surface parallel to the flow direction. The CFD results over the tab are also of lower reliability as the assumption of a linear decay in the data correction may need refinement.

The pressure distributions predicted from CFD analysis use a number of sample locations at which the pressure is recorded. Numerical integration of these pressures over the length of the hull provides a result for the total lift force generated by the stern tab deflection. The same pressure integration technique can be applied to the experimental pressure measurements, albeit using a data set with lower resolution. The numerically integrated lift force magnitudes from CFD analysis are compared in Figure 15 with the model scale integrated pressure measurements and the directly measured total force magnitudes made by Arnold [6]. The force testing results were obtained using strain gauge measurements of the bending moment at two different locations on the aft hull mountings, from which the resultant force could be calculated.

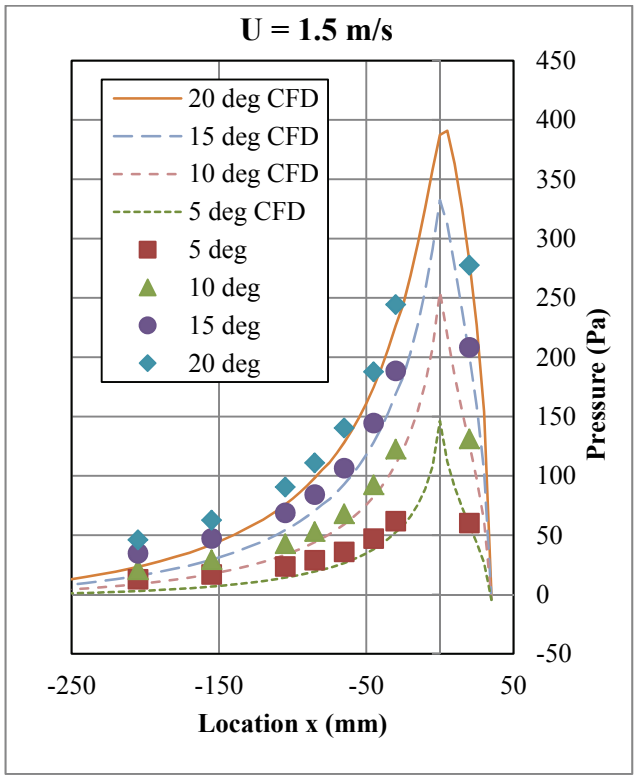

Figure 11: Hull underside pressure distributions at U = 1.5 m/s as a function of tab angle. Markers represent experimental values, lines represent CFD values.

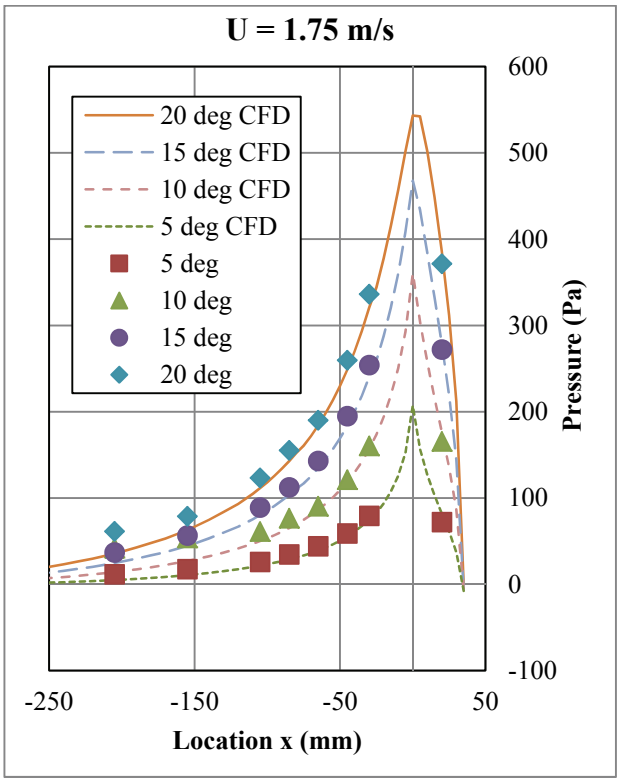

Figure 12: Hull underside pressure distributions at U = 1.75 m/s as a function of tab angle. Markers represent experimental values, lines represent CFD values.

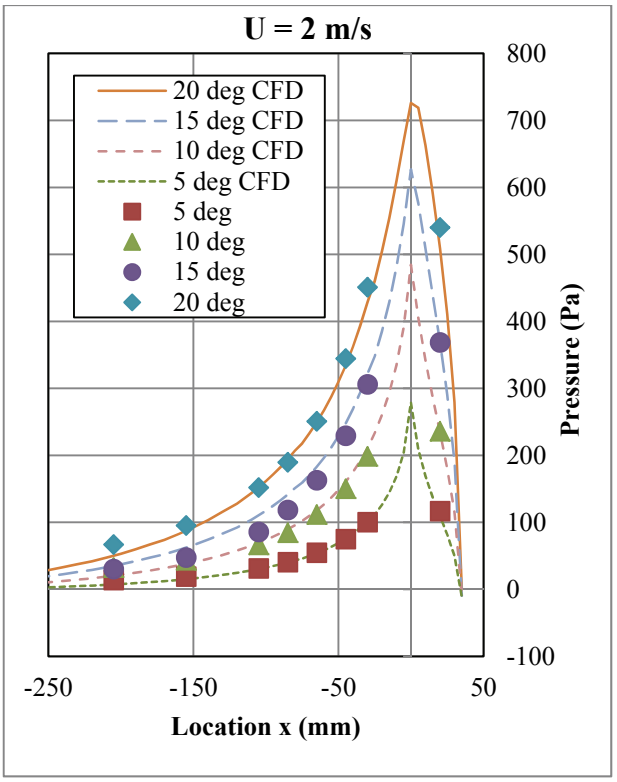

Figure 13: Hull underside pressure distributions at U = 2 m/s as a function of tab angle. Markers represent experimental values, lines represent CFD values.

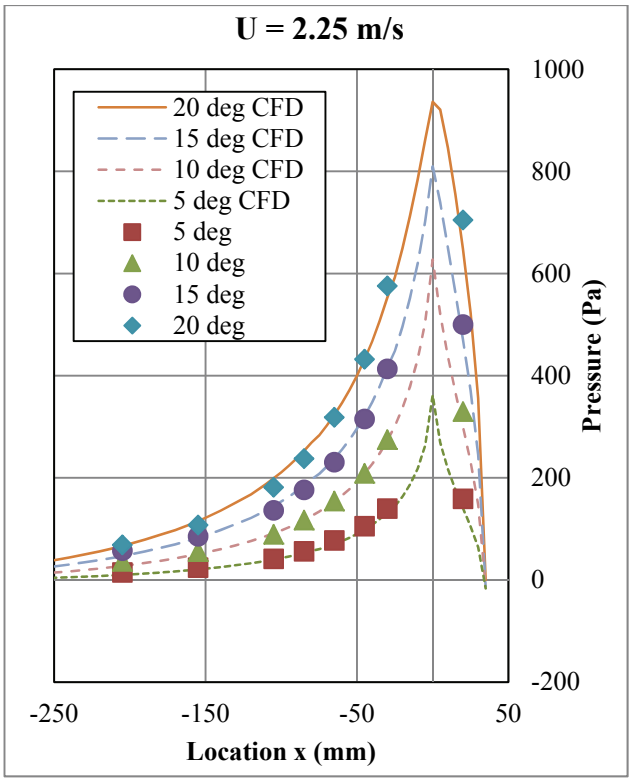

Figure 14: Hull underside pressure distributions at U = 2.25 m/s as a function of tab angle. Markers represent experimental values, lines represent CFD values.

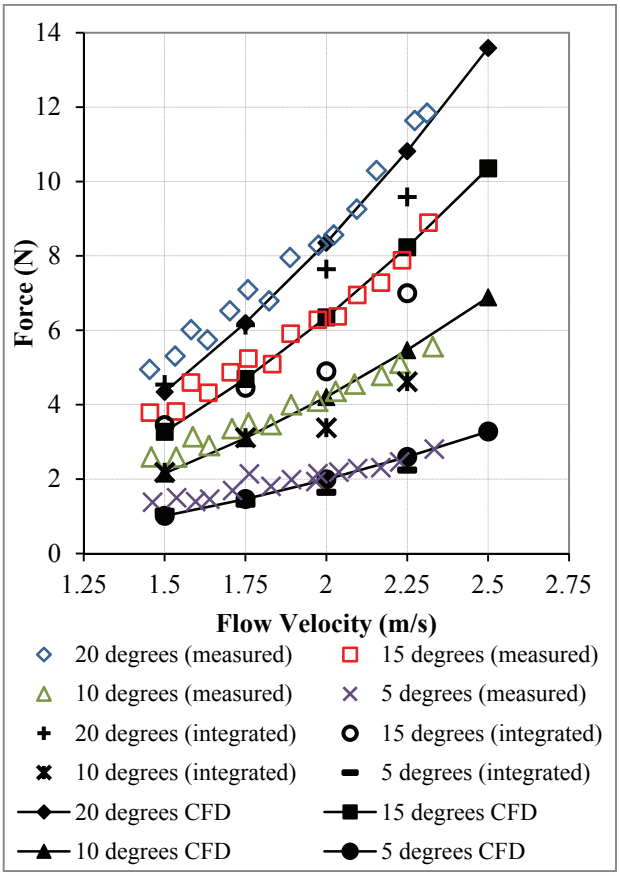

Figure 15: Comparison of total lift force from total force test data [6] with integrated lift force from CFD and from measured pressure distributions.

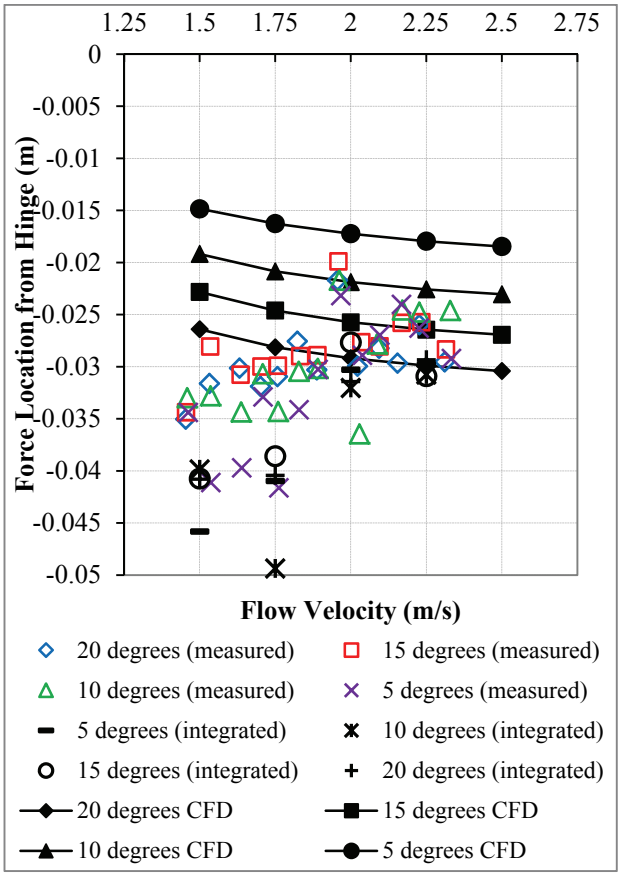

Figure 16: Comparison of resultant force locations from force testing [6], integration of pressure testing and CFD.

The numerical integration of the pressure measurements is approximate as it does not involve high resolution around the tab hinge and hence contribution of the peak pressure region is not well represented in the integration. This is an inevitable consequence of the difficulty of making pressure measurements on such a small model. This underestimation of the resultant force magnitude is somewhat compensated for by the measurement of only the centreline pressures, which will be where the maximum pressure occurs at each streamwise location. For integration purposes, the zero pressure point on the hull was assumed to be 300 mm forward of the tab hinge.

The location of the resultant lift force (that is the centre of pressure) is shown in Figure 16 which compares results from the three methods. The CFD and force testing results are in closer agreement at higher flow velocities. All methods of analysis show that the centre of pressure is located substantially forward of the tab hinge.

6. CONCLUSIONS

The CFD and testing results are in close agreement at model scale, which essentially validates the CFD methodology to the extent that the two dimensional CFD solution is a good simulation of the pressure distribution at the model centre line. The results indicate that the maximum pressure occurs in the vicinity of the tab hinge and that the pressure distribution is long-tailed in the direction forward of the hinge. This explains why the resultant lift force due to stern tab deflection is located forward of the tab [15]. Subsequently, most of the trim moment produced on the ship is due to the increase in pressure forward of the tab rather than the actual forces acting on the tab.

Better understanding of these loads and their distribution assists in the use of stern tabs as a form of ride control, as the exerted trim moment can be estimated with more confidence. These results also provide a more detailed assessment of the structural loads on the ship due to trim tab deflection than has previously been available. This pressure distribution and the resulting structural stresses may then be optimised by altering the geometry of the stern tabs.

There is scope for further experimental investigation into a more detailed study of the pressures in the vicinity of the tab hinge and on the tab. This would provide additional information for the refinement of the two-dimensional CFD data analysis. Furthermore, a three-dimensional CFD model would be beneficial to a more conclusive verification of the two-dimensional analysis and the experimental data. Testing and CFD analysis at full scale would also provide a useful comparison with the extrapolated model scale data.

7. REFERENCES

1. K. FUKUNAGA, Y. IKEDA, AND Y. NIHEI, An experimental study on the seakeeping characteristics of a fast wave-piercing catamaran in real seas, *Journal of the Japan Society of Naval Architects, Volume 8, pp 107-114,* 2008.
2. J. GERRITSMA AND W. BEUKELMAN, The distribution of the hydrodynamic forces on a heaving and pitching shipmodel in still water, *5th Symposium on Naval Hydrodynamics Ship Motions and Drag Reduction, pp 219-246,* 1964.
3. J.-F. TSAI, J.-L. HWANG, S.-W. CHAU, AND S.-K. CHOU, Study of hydrofoil assistance arrangement for catamaran with stern flap and interceptor, *6th International Conference on Fast Sea Transportation, FAST '01, pp 69-78,* 2001.
4. T. W. WATSON, High-speed ship-model extrapolation, Honors Thesis, *Australian Maritime College,* 2007.
5. J. BELL, Measured loads response of motion controls on an INCAT catamaran model, Honours Thesis, *School of Engineering, University of Tasmania,* 2011.
6. T. ARNOLD, Model scale analysis of the loads response due to stern tabs on an INCAT catamaran, Honours Thesis, *School of Engineering, University of Tasmania,* 2012.
7. M. GUPTA, M. MCCAIN, and D. EISELE, A route or mission-dependent approach for the calculation of rational structural dynamic loads for high-speed multihulls, *Society of Naval Architects and Marine Engineers,* 2003.
8. M. R. DAVIS and D. S. HOLLOWAY, Motion and passenger discomfort on high speed catamarans in oblique seas, *International Ship Building Progress, Vol 50 (4), pp 333-370,* 2003.
9. J. LAVROFF, The slamming and whipping response of a hydroelastic segmented catamaran model, PhD, *School of Engineering, University of Tasmania,* 2009.
10. G. THOMAS, Wave slam response of large high speed catamarans, PhD, *School of Engineering, University of Tasmania,* 2003.
11. M. R. DAVIS, G. THOMAS, D. S. HOLLOWAY, J. LAVROFF, W. AMIN, S. MATSUBARA, and T. R. ROBERTS, Slamming and whipping of wave-piercing catamarans, *5th International Conference on Hydroelasticity in Marine Technology, pp on CD,* 2009.
12. D. SRIDHAR, T. V. K. BHANUPRAKASH, and H. N. BDAS, Frictional resistance calculations on a ship using CFD, *International Journal of Computer Applications,* vol. 11, 2010.

13. A. BARTON, Friction, Roughness and boundary layer characteristics of freshwater biofilms in hydraulic conduits, PhD, *School of Engineering, University of Tasmania,* 2007.
14. ANSYS, ANSYS CFX-Solver Theory Guide, 2009.
15. J. BELL, T. ARNOLD, J. LAVROFF, M. R. DAVIS, Measured Loading Response of Model Motion Control Stern Tabs, *International Journal of Maritime Engineering, vol. 155, Part A1, pp 1 - 7,* 2013.